Desalination and Water Treatment
www.deswater.com
doi: 10.5004/dwt.2022.28366

256 (2022) 253–264
April

Kinetic and equilibrium studies of the activated carbon prepared from jackfruit leaves for the adsorption of methyl orange

Muhammad Zobayer Bin Mukhlish, Shafiul Hossain, Md Anisur Rahman, Md. Tamez Uddin*

Department of Chemical Engineering and Polymer Science, Shahjalal University of Science and Technology, Sylhet 3114, Bangladesh, Tel. +880 821 717850, Ext 681; Fax: +880 821 715257; email: mtuddin_cep@yahoo.com (Md. Tamez Uddin)
ORCID: 0000-0001-9235-1112

Received 21 June 2021; Accepted 2 March 2022

ABSTRACT

In the present study, activated carbon (AC) was prepared from jackfruit leaves (JFL) using phosphoric acid as activating agent. The prepared AC was characterized by Fourier-transform infrared spectroscopy, nitrogen adsorption–desorption analyses and scanning electron microscopy. The adsorptive performance of the prepared activated was investigated by the adsorption of anionic dye methyl orange (MO) from aqueous solutions. The batch adsorption experiments were carried by varying operation parameters such as pH, adsorbent dosage, initial concentration of dye and contact time. The adsorption capacity was increased with increasing concentration of dye. The equilibrium adsorption data were well fitted to Langmuir isotherm model and maximum adsorption capacity was obtained to be 833 mg/g. The adsorption followed the pseudo-second-order kinetic model. Thermodynamic study suggested the endothermic nature of MO adsorption onto prepared activated carbon. Considering high dye adsorption capacity, AC prepared from jackfruit leaves can be used as a promising low-cost adsorbent for the removal of organic dyes from aqueous solution.

Keywords: Jackfruit leaves; Activated carbon; Adsorption; Isotherm; Kinetics

1. Introduction

Dyes are widely used in textiles, paints, leather, papers, pharmaceutical, food, cosmetics, plastics, and photographic industries [1]. Most industrial dyes are toxic, carcinogenic, and mutagenic and may cause severe damage to human beings, such as dysfunction of the kidneys, reproductive system, liver, brain and central nervous system [2]. Moreover, dye-containing effluents are highly colored, so discharging these dye containing effluents into natural water bodies affects the balance of aquatic ecosystems because they prevent the transmission of sunlight through water, which results in a reduction in dissolved oxygen content [3]. Among the synthetic dyes, anionic azo dyes constitute about 60%–70% of the dye synthesis and industrial use. In addition, synthetic azo dyes are known as carcinogenic, teratogenic and mutagenic organic substances and pose a potential threat to aquatic organisms as well as human life [4–9]. Azo dyes can be accumulated in agricultural soil during irrigation with azo dye containing wastewater. These azo substances are detrimental to soil microbial communities and to germination and growth of crops [10,11]. Methyl orange (MO), a prominent azo anionic dye, is harmful to the environment, organisms and human. Intake of MO can cause adverse health effects on human such as vomiting, diarrhea and intestinal cancer. Moreover, excessive levels of MO ingestion can even lead to death [12,13]. Therefore, wastewater containing such ecotoxic dye should be treated properly prior to discharge into aquatic ecosystem or carry out secondary use. Hence, it is prerequisite to develop an

* Corresponding author.

effective process that can effectively treat these dye containing wastewaters.

The possible methods of dye removal from industrial effluents include adsorption [14–16], chemical coagulation [17], flocculation [18], advanced chemical oxidation [19–21], froth floatation [22], ozonation [23], reverse osmosis [24,25] and biological techniques [26,27]. Although the above-mentioned physical and /or chemical methods have been widely used, they possess inherent limitations such as high cost, formation of hazardous by-products and intensive energy requirements. Therefore, the development of newer eco-friendly methods to treat these pollutants became an imperative task. Adsorption has been found to one of the most widely used methods for dye removal because of its low cost, simplicity, high efficiency, and easy operation [2,14,28–30]. Different adsorbents such as halloysite nanotubes and chrysotile nanotubes [8], cetyltrimethyl ammonium bromide modified cellulose [31], Ce(III)-doped UiO-66 [32], lala clam shell [13], bentonite [33], and bottom ash and de-oiled soya [12], kahwa tea (*Camellia sinensis*) carbon [29], ordered mesoporous carbon [34], guar gum/activated carbon nanocomposite [35], black turmeric rhizome ash [36] and layered double hydroxides [29] have been tested to remove MO or other organic dyes from aqueous solution.

Liquid phase adsorption using activated carbon (AC) is one of the popular methods for the removal of pollutants from wastewater due to its effectiveness and versatility. However, the cost limits widespread use of AC. This fact has prompted a growing interest into the production of low-cost AC. But, the main challenge in the manufacture of commercial ACs is to identify new precursors that are cheap, accessible and available in abundant quantity which has potential for significant economic benefits. Up to now, great efforts has been made in finding the low-cost precursors including agricultural by-products, industrial wastes and biological materials [37]. Among them, agricultural by-products have been proved to be a promising raw material for the production of AC because of their features-availability at a low price, considerable mechanical strength, and low ash content [38,39]. Many attempts have been made to obtain ACs from agricultural wastes including coconut shells [40], rice husk [41], olive stone [42], hazelnut shell [43], cauliflower waste [44], peanut hull [45], sugar cane bagasse [46], date pits [47], bamboo [48], jackfruit peel [49], sugarcane bagasse [50] etc. However, the properties of AC depend on the type of precursors. Among the agricultural wastes, jackfruit leaf might be one of the best alternatives for the preparation of AC. Jackfruit is a tropical plant whose leaf is available all over the year in Bangladesh. The adsorption capacity of jackfruit leaf powder for the removal of methylene blue has been investigated in our previous study [28,51]. Adsorption performances of the AC prepared from jackfruit peel have been studied for the removal of phenol and chlorophenols [52], basic dyes [53] and Cd(II) [54] from aqueous solutions. However, no systematic experiment has ever been performed to use jackfruit leaf as low-cost precursor to prepare AC for the removal of anionic dye methyl orange (MO) from aqueous solutions.

In this study, the potentiality of the AC prepared from jackfruit leaf (JFL) for the removal of MO was studied. The AC was prepared by chemical activation using phosphoric acid as the activating agent. Batch adsorption studies were performed using MO as a model dye in order to investigate adsorption performance of the prepared AC. Effect of solution pH, MO concentration and contact time on the adsorption of MO onto the AC was examined. The prepared AC was characterized with scanning electron microscopy (SEM), pH_{ZPC} and Fourier-transform infrared spectroscopy (FTIR) techniques. The textural characterization of the prepared AC was also carried out. The equilibrium and kinetic data were evaluated in order to explore the adsorption mechanism of MO onto AC.

2. Materials and methods

2.1. Preparation of AC

Jackfruit leaves were collected from local areas in Sylhet and thoroughly washed with distilled water for several times to remove dirt and earthy materials followed by drying at 100°C in a hot air oven (Memmert, Model: 500) for 12 h. The dried leaves were crushed into powder with a blend and sieved to desired particle size. The as-prepared leaf powder was then impregnated with 85% phosphoric acid at 1:3 ratio. Subsequently, the impregnated powder was separated by filtration and dried in oven at 120°C for 24 h. Subsequently, the impregnated precursor (of known weight) is transferred to locally made stainless steel reactor (18 cm length and 4.5 cm diameter) with narrow ports at both ends. Nitrogen (N_2) gas was purged through the reactor to create an inert atmosphere inside the reactor. After purging, both ends of reactor were closed and the reactor was placed inside a muffle furnace for carbonization at a temperature of 600°C and holding time of 4 h. The samples were then cooled to room temperature followed by washing with distilled water for several times until the pH of the washing solution reached 7. Finally, the samples were dried in an oven at 105°C for 24 h and then stored in an air tight container.

The cost estimates for laboratory-scale production were generated on the basis of 100 g ACs produced by chemical activation of JFL powder in the laboratory. The raw jackfruit leaves was obtained from plantation and utilized as starting materials for the production of AC. Hence, the purchased price of the raw jackfruit leaves was not included in the cost study. The cost for consumables was obtained from budgeting consumable quotations received from suppliers. Utility requirements were determined using industrial electricity pricing from the local electricity source (Bangladesh Power Development Board (BPDB), Sylhet). The main power consuming equipment are drying oven and electric furnace. The production cost of activated carbon from JFL obtained by chemical activation by phosphoric acid was calculated to be USD 2.58/kg.

2.2. Preparation of dye solutions

Analytical grade methyl orange (MO) (Merck, Germany) was used as a model dye for this experiment. Stock solution of 1,000 mg/L MO was prepared by dissolving 1 g MO in 1 L of distilled water. The as-prepared stock solution was

further diluted to desired extent to obtain the test solution of desired concentration. pH of the solutions was adjusted using 0.1 M NaOH and 0.1 M HCl solutions.

2.3. Characterization of adsorbent

Nitrogen (N_2) gas adsorption–desorption isotherm of the prepared AC was carried out to investigate the textural characteristics as specific area, pore size and pore volume. The N_2 adsorption was carried out at 77 K using an automatic Micromeritics ASAP-2020 volumetric sorption analyzer. The samples were first degassed at 120°C in vacuum in order to reach a constant pressure (<10 μm Hg). The Brunauer–Emmett–Teller (BET) equation in the relative pressure (P/P_0) range of 0.06–0.3 was employed to calculate the BET specific area (S_{BET}). Mesopore size distributions were deduced from the Barrett, Joyner, Halenda (BJH) method applied to the adsorption branch of the nitrogen adsorption isotherm. The calculation was performed by the Micromeritics software package which uses the recurrent method and applies the Harkins and Jura equation for the multilayer thickness. Scanning electron microscopy (SEM) analysis was carried out for the prepared AC to study their surface textures and the development of porosity. FTIR analysis was carried out to determine the surface functional groups using FTIR spectroscope (IRPrestige-21, Shimadzu, Kyoto, Japan). Samples were diluted with KBr and pressed into a disk shape prior to FTIR analysis. FTIR spectra were recorded in the range of 450–4,000 cm^{-1}. Point of zero charge, pH_{PZC} of adsorbent was determined by pH drift method [55]. 0.10 g of adsorbent was introduced in different Erlenmeyer flask of 250 mL containing 200 mL of 0.01 M NaCl solution. pH values of the solutions were adjusted in the range of 2–11 by adding 0.1 N NaOH and 0.1 N HCl solution. These flasks were then shaken in a flask shaker machine (Model: SF1, Stuart Scientific Co. Ltd., UK) at constant oscillation of 300 osc/min for 48 h and the final pH of the solutions were measured by a pH meter (Model: HI2211, HANNA Instruments, Singapore). The point of intersection of the plot of pH_{final}–$pH_{initial}$ vs. $pH_{initial}$ was recorded as pH_{PZC} of JFL AC adsorbent.

2.4. Adsorption study

The effect of different parameters such as pH, initial concentration and contact time was determined by batch studies. In each case, a known concentration of dye solution of 200 mL was brought into contact with a predetermined amount of AC in a 250 mL plastic Erlenmeyer flask and the obtained solution was kept in agitation using a flask shaker at a constant oscillation of 350 osc/min for 6 h. Preliminary studies showed that there was no significant change in dye uptake after a contact time of 6 h and hence, the contact time was kept fixed at 360 min for all the batch experiments. All the experimental runs were carried out at room temperature (28°G). After attaining equilibrium, the samples were centrifuged using a centrifuge machine (Model: DSC-200A-2, Digisystem laboratory Instruments Inc., Taiwan) at 4000 rpm for 10 min and the concentrations of the supernatant MO solutions were obtained by measuring absorbance at the wavelength of 464 nm using UV-Vis spectrophotometer (Model: UV-2600, Shimadzu, Kyoto, Japan). The amount of dye adsorbed on to the adsorbent at equilibrium, q_e (mg/g) was calculated by the following expression:

$$q_e = \frac{(C_0 - C_e)V}{W} \tag{1}$$

where C_0 (mg/L) and C_e (mg/L) are the liquid phase concentration of dye at initial and equilibrium respectively. V is the volume of the solution in liters and W is the mass of the dry adsorbent in gram.

In a similar way, the effect of pH was studied using 100 mg/L MO solution with adsorbent mass of 0.1 g in the pH range of 2–11. Absorbance of MO solutions of varying pH was analyzed by the UV-Vis spectrophotometer before carrying the experiment and no appreciable change was found. Equilibrium isotherm studies were also carried out in a same way taking solutions of different initial concentrations (100, 200, 250 and 300 mg/L) of 200 mL in different Erlenmeyer flasks with 0.1 g adsorbent. The effect of contact time as well as the adsorption kinetics experiment were done for four MO solutions of different initial concentrations (100, 200, 250 and 300 mg/L) of same volume with same amount of adsorbent as before. Samples were pipetted out at different time intervals, centrifuged and then the concentration in the supernatant solution was analyzed as before. The amount of dye adsorbed q_t (mg/g) at time t was calculated by the following equation:

$$q_t = \frac{(C_0 - C_t)V}{W} \tag{2}$$

where C_t (mg/L) is the liquid phase concentration of dye solution at time t.

Two famous models- namely Langmuir and Freundlich models were used to study the equilibrium sorption process. Langmuir isotherm model which assumes monolayer adsorption on a structurally homogeneous and energetically equivalent adsorbent sites with no interaction between the adsorbed molecules was used to estimate maximum adsorption capacity [56]. The linearized form of Langmuir equation can be written as:

$$\frac{C_e}{q_e} = \frac{1}{K_L q_{\max}} + \frac{C_e}{q_{\max}} \tag{3}$$

where q_e is the adsorbed amount of dye per unit adsorbent at equilibrium (mg/g), C_e is the equilibrium concentration of the dye in the solution (mg/L), $q_{\max}$ is the maximum monolayer adsorption capacity (mg/g) and K_L is the constant related to the free energy of adsorption (L/mg). The values of $q_{\max}$ and K_L can be calculated from the slope and intercept of the linear plots of C_e/q_e vs. C_e.

Freundlich isotherm model [57] is an empirical equation which considers that the adsorption process takes place on heterogeneous and energetically nonequivalent surface with infinite surface coverage, and adsorption capacity appears to be directly related to the concentration of dye at equilibrium. The well-known linearized form of Freundlich isotherm can be expressed as:

$$\ln q_e = \ln K_F + \frac{1}{n}\ln C_e \tag{4}$$

where K_F (mg/g(mg/L)$^{1/n}$) is the Freundlich isotherm constant, which is an indicative of the extent of adsorption (i.e., adsorption capacity) and n (dimensionless) is a measure of the adsorption intensity or surface heterogeneity that represents bond distribution (a value closer to zero represents more heterogeneous surface). A value of $1/n < 1$ indicates a normal Langmuir isotherm, while $1/n > 1$ is indicative of cooperative adsorption [58]. The values of n and K_F are calculated from the slope and intercept of the linear plot of $\ln q_e$ vs. $\ln C_e$.

To describe the kinetics of adsorption, the pseudo-first-order model [59] and the pseudo-second-order model [60] are mostly used by the researchers. The linearized-integral form of the most popular pseudo-first-order model by Lagergren is:

$$\ln\left(q_e - q_t\right) = \ln q_e - k_1 t \tag{5}$$

The integrated form of the pseudo-second-order model can be linearized as:

$$\frac{t}{q_t} = \frac{1}{k_2 q_e} + \frac{t}{q_e} \tag{6}$$

where q_e and q_t are the adsorption capacity in mg/g at equilibrium and at time t (min) respectively. k_1 (min^{-1}) is the rate constant of pseudo-first-order sorption, k_2 (g/mg-min) is the rate constant of pseudo-second-order sorption, and h (mg/g min) represents the initial adsorption rate.

A plot of $\ln(q_e - q_t)$ against t should give a linear relationship if the kinetic data follows pseudo-first-order kinetics. The values of k_1 and q_e can be calculated from the slope and intercept of the obtained straight line. A linear plot of t/q_t vs. t confirms the conformity of the kinetic data to the pseudo-second-order kinetics. The slope and intercept of the straight line are used to calculate the value of q_e and k_2 respectively.

Besides the value of R^2, the suitability of the models is verified by applying error analysis function Chi-square test (χ^2), formula of which is as follow:

$$\chi^2 = \sum \frac{\left(q_{e_{\text{exp}}} - q_{e_{\text{model}}}\right)^2}{q_{e_{\text{model}}}} \tag{7}$$

where $q_{e_{\text{exp}}}$ (mg/g) and $q_{e_{\text{model}}}$ (mg/g) are experimental and model value of the adsorption capacity.

3. Results and discussions

3.1. Characterization of AC

FTIR spectroscopy is a powerful characterization technique for the functional group analysis. The FTIR analysis of JFL AC was conducted before and after adsorption of MO, and the as-obtained two spectra were compared to reveal whether there were changes in the spectrum due to adsorption of MO. The FTIR spectra obtained for AC before and after MO adsorption are shown in Figs. S1a and b, respectively. In Fig. S1a, the broad band appeared at 3,500–3,700; 3,250; 2,918; 2,360; 1,575; 1,274 and 968 cm^{-1} could be due to the –OH stretching, –CH_2– stretching, C≡C stretching, C=C stretching, =C–O–C stretching and C=C bending vibration, respectively [61]. As compared with the FTIR spectrum of JFL AC (Fig. S1a), the new peaks observed at 1,462 and 1,205 cm^{-1} in the spectrum of JFL AC after adsorption of MO (Fig. S1b) are indicative of –N=N– band stretching and –SO_3 stretching vibrations [62,63]. The peak of C=C bending of alkene is shifted from 968 to 866 cm^{-1} after adsorption of MO. From the above discussion it can be concluded that the disappearance, shifting and the appearance of new peak indicated the adsorption of MO onto JFL AC.

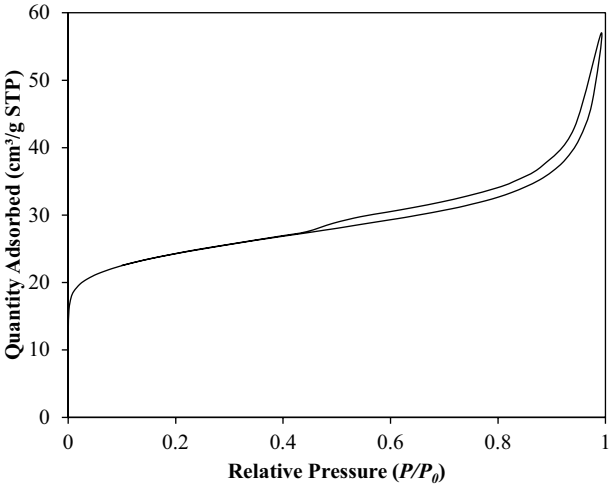

Fig. 1. Nitrogen adsorption–desorption isotherm at 77 K on JFL AC.

The textural property of the as-prepared AC was studied by N_2 sorption measurement at liquid N_2 temperature. Fig. 1 shows the nitrogen adsorption–desorption isotherm of the AC. The isotherm of the prepared AC revealed a typical type IV sorption behavior including a type H4 hysteresis loop which is typical of mesoporous materials, according to the IUPAC classification [64]. The Brunauer–Emmett–Teller (BET) specific surface area, the pore size and the total pore volume of JFL AC were determined by Barrett–Joyner–Halenda (BJH) method [65]. The JFL AC exhibited a BET surface area of 81.45 m^2/g with adsorption and desorption average pore diameter of 4.23 and 3.43 nm, respectively. BJH adsorption and desorption cumulative pore volume were 0.0624 and 0.0625 cm^3/g, respectively.

The porous structure of the prepared AC was further confirmed by scanning electron micrographs (SEM) as shown in Fig. 2. From Fig. 2 it is seen that the ACs were in the form of spherical shaped particles that aggregated together to form pieces with different sizes.

3.2. Adsorption study

3.2.1. Effect of dosage

The effect of adsorbent dosage on the uptake of MO by JFL AC was studied. Fig. 3 shows the effect of adsorbent

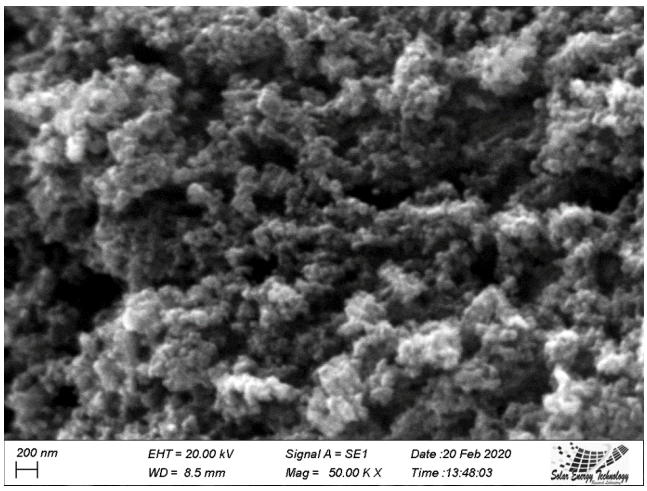

Fig. 2. Scanning electron micrograph of AC prepared from JFL.

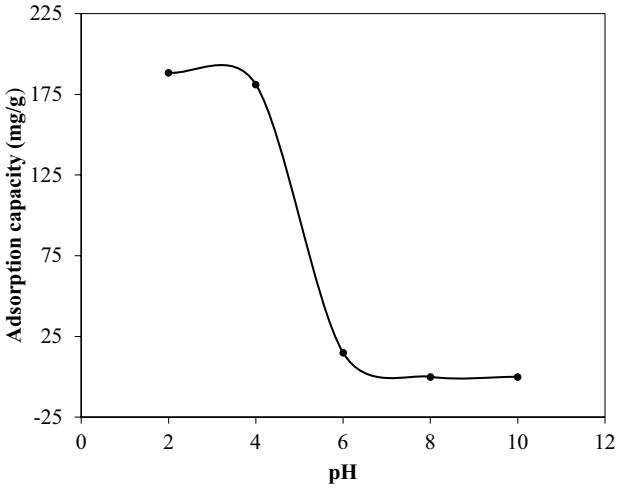

Fig. 4. Effect of pH on the adsorption of MO onto JFL AC.

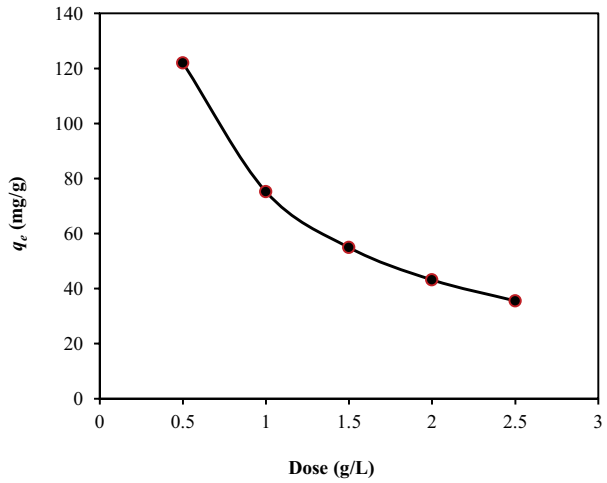

Fig. 3. Effect of adsorbent dosage on the MO sorption onto JFL AC (C_0 = 100 mg/L, dose = 0.5–2.5 g/L, V = 200 mL, T = 28°C).

dosage on the sorption of MO dye. As shown in Fig. 3, the adsorption capacity (q_e) decreases with increasing adsorbent dosage. This may be due to the split in the flux or the concentration gradient between dye concentration in the solution and the dye concentration on the surface of the JFL [2,5]. Similar behavior has been reported in case of adsorption of reactive red 120 dye onto alumina-silica nanofiber [6], methylene blue onto jackfruit leaf powder [66] and tartrazine and sunset yellow anionic dyes onto activated carbon [67].

3.2.2. Effect of pH

Adsorption capacity is highly dependent on the surface charge of adsorbent and the nature of dye molecule which are largely controlled by solution pH. Hence, solution pH plays a dominant role in defining adsorption capacity of an adsorbent. Fig. 4 shows the effect of initial pH on the adsorption capacity of JFL AC for the adsorption of MO. From Fig. 4, it was clear that adsorption of MO on the JFL AC was favorable at lower pH. The highest adsorption capacity was obtained at pH 3 and the adsorption capacity was suddenly decreased after pH 4. This behavior can be well described by taking into consideration the pH_{PZC} value 4.2 (Fig. S2) below which surface charge of the AC becomes positive and above which surface charge becomes negative. Therefore, at a pH value lower than 4.2, an increased electrostatic attraction between the positive charged surface and the anionic dye molecule was expected leading to increased adsorption density. In contrast, above pH 4.2, the adsorbent surface became negatively charged which repelled anionic dye molecules, contributing to decreased adsorption capacity. This behavior over pH change is quite similar to previous studies reported elsewhere [12,68].

3.2.3. Effect of contact time and initial dye concentration

The variation in the adsorption capacity (q_t) with contact time at different initial concentrations ranging from 100 to 300 mg/L is shown in Fig. 5. Dye uptake was rapid for the first 40 min, and then proceeded at a slower rate and finally attained equilibrium after which the amount of dye adsorbed was negligible. The fast adsorption rate at the initial stage resulted from the higher concentration gradient existed between methyl orange concentration in the bulk and the vacant site on the AC. As the time proceeded, the concentration of dye in the bulk phase decreased and the vacant site on the AC was occupied by dye molecules which decreased concentration gradient leading to the slow adsorption rate at the later stages. The amount of methyl orange adsorbed per unit mass of AC at equilibrium, that is, the equilibrium adsorption capacity of AC (q_e) was increased with increasing initial dye concentrations. As the initial concentration of dye increased from 100 to 300 mg/L, the equilibrium adsorption capacity of AC was increased from 140 to 318 mg/g. This was due to increase in the driving force of the concentration gradient at higher initial dye concentration. When the initial concentrations were increased, the mass transfer driving force became larger resulting in higher adsorption capacity [2].

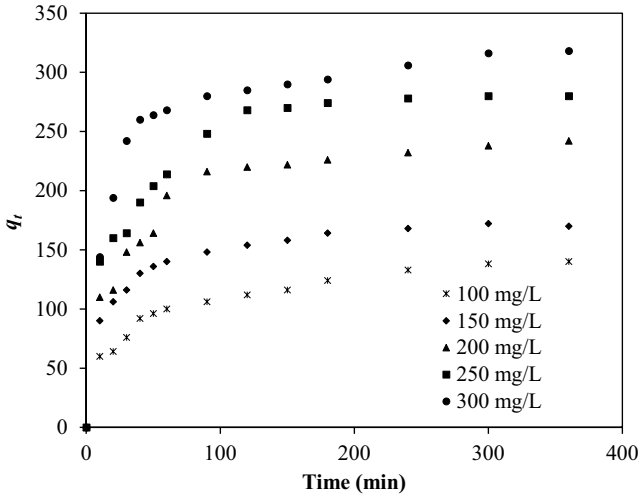

Fig. 5. Effect of initial concentration and contact time on the adsorption of MO onto JFL AC (C_0 = 100, 150, 200, 250 and 300 mg/L, W = 0.1 g, V = 200 mL, T = 28°C).

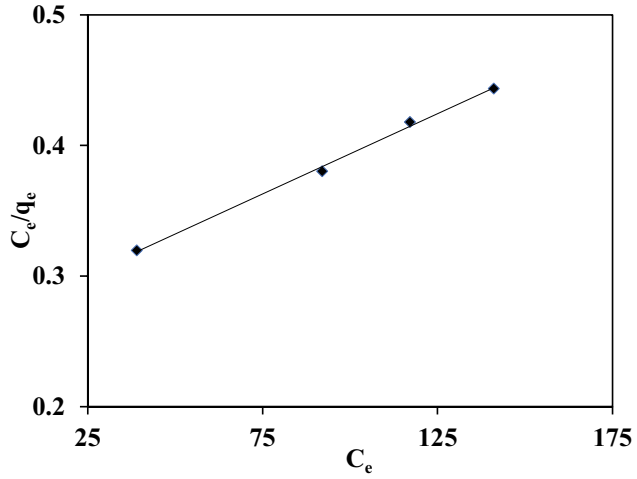

Fig. 6. Langmuir isotherm for adsorption of MO on JFL AC adsorbent (C_0 = 100, 200, 250 and 300 mg/L, W = 0.1 g, V = 200 mL, T = 28°C).

3.2.4. Adsorption isotherms

Equilibrium dependency of the amount of dye adsorbed on its liquid phase concentration at constant temperature is known as adsorption isotherm an important parameter to estimate the adsorbate–adsorbent interaction, which is critical in optimizing the required amount of adsorbent for a certain degree of removal and also for designing an adsorption system. To describe the equilibrium adsorption process fitting of the isotherm data to different isotherm models is considered as a crucial step. Hence, the experimental data were fitted to Langmuir model [Eq. (3)] and Freundlich model [Eq. (4)], and the corresponding plots are shown in Fig. 6 and Fig. S3, respectively.

The correlation coefficients (R^2) for Langmuir and Freundlich isotherms obtained from the application of the models using Eqs. (3) and (4) were 0.9970 and 0.9976, respectively. The values of model parameters as well as correlation coefficient (R^2) are presented in Table 1. As shown in Table 1, the values of R^2 are close to unity for both Langmuir and Freundlich isotherm models. However, the value of $1/n$ in Freundlich isotherm is smaller than unity and this indicates that the adsorption equilibrium data follows Langmuir isotherm model. As estimated from Langmuir model, the maximum monolayer adsorption capacity of JFL AC was 833 mg dye/g adsorbent. The adsorption capacity of various adsorbents for the removal of methyl orange are reported and compared with that of the present study in Table 2. It was observed that the maximum adsorption capacity, that is, the equivalent total adsorption site of JFL AC adsorbent for the removal of MO was significantly higher than many other low cost bio materials investigated so far. Therefore, JFL AC can be effectively used for treating MO contaminated wastewater.

3.2.5. Kinetic studies

The study of adsorption kinetics is very important in order to observe the controlling step of dye adsorption from aqueous solution. The sorption dynamics of MO by JFL AC was examined with the pseudo-first-order and pseudo-second-order kinetic model. The linear plots of $\ln(q_e - q_t)$ vs. t and t/q_t vs. t for the pseudo-first-order and pseudo-second-order kinetic model for the adsorption of MO onto prepared AC are shown in Fig. S4 and Fig. 7, respectively. The calculated value of k_1, k_2, q_e and their corresponding regression coefficient values (R^2) are presented in Table 3. Table 3 clearly shows that the calculated q_e values were found to be much closer to the experimental data (q_{exp}) for the pseudo-second-order kinetic model. The correlation coefficients (R^2) were also closer to unity for pseudo--second-order kinetics than for pseudo-first-order kinetics. Besides the value of R^2, the suitability of the models was verified by applying error analysis function Chi-square test (χ^2). These suggested that the adsorption system could be better represented by the pseudo-second-order model.

Table 1
Langmuir and Freundlich isotherm parameters and correlation coefficients for the adsorption of MO on JFL AC

Langmuir isotherm			Freundlich isotherm		
q_{max} (mg/g)	K_L (L/mg)	R^2	K_F (mg/g(mg/L)$^{1/n}$)	$1/n$	R^2
833	0.004	0.9970	7.858	0.7512	0.9976

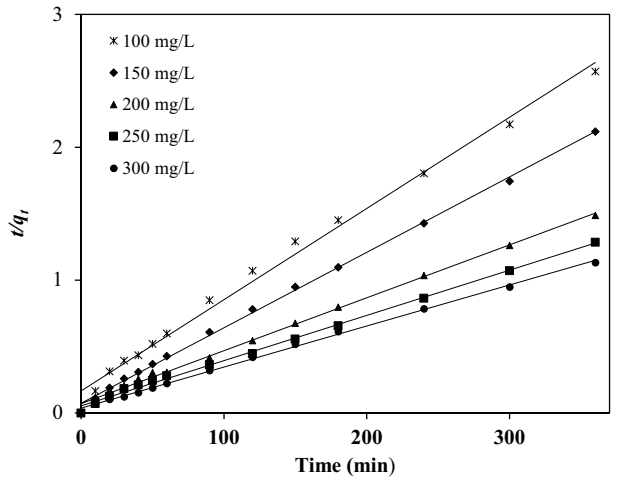

Fig. 7. Pseudo-second-order kinetic plot for the adsorption of MO onto JFL AC.

3.2.6. Proposed adsorption mechanism

The mechanism of dye adsorption onto adsorbents must be understood in order to remove dyes from textile wastewaters effectively. The electrostatic interaction between the positively charged surface of JFL AC and the negatively charged MO dye can be used to explain the MB adsorption mechanism. The adsorbent's surface functional groups and the pH dependent adsorption of MO onto the adsorbent can elucidate this electrostatic interaction. FTIR measurements revealed the presence of hydroxyl groups on the JFL AC surface. The ionization of these groups, which is dependent on the pH of the solution, leads in an electrical charge on the surface of the JFL AC adsorbent. Depending on pH, the hydroxyl groups on the surface of AC can either accept or lose a proton, causing the surface charge to change.

AC's surface may become negatively charged at high pH when hydroxyl groups react with OH^- (deprotonation reaction), as indicated in Eq. (8).

$$\text{AC-OH} + \text{OH}^- \rightarrow \text{AC-O}^- + \text{H}_2\text{O} \tag{8}$$

Thus, a force of repulsion occurs between the dye anions and the negatively charged adsorbent surface. On the other hand, when the pH of the solution is low, the AC surface sites are protonated and become positively charged, as depicted in Eq. (9).

$$\text{AC-OH} + \text{H}^+ \rightarrow \text{AC-OH}_2^+ \tag{9}$$

Thus, at low pH, the adsorption process was highly favored through the electrostatic forces of attraction as proposed in Eq. (10).

$$\text{AC-OH}_2^+ + \text{MO} \rightarrow \text{AC-OH}_2^+ \cdots \text{MO} \tag{10}$$

The adsorption of MO by electrostatic attraction was evidenced by desorption study which is discussed in the following section.

3.2.7. Desorption and reusability studies

Desorption study was conducted to investigate the reusability of adsorbent and the possibility of dye recovery

Table 2
Comparison of maximum monolayer adsorption capacity of various AC and bioadsorbents

Adsorbent	Adsorption capacity, q_{max} (mg/g)	References
Coffee grounds AC	658	[69]
Phragmites australis AC	217	[70]
Pinecone AC	404	[71]
Finger-citron-residue AC	934	[72]
Date pit AC	434	[73]
Shaddock peels AC	94	[74]
Date stones AC	3.0	[75]
Pomelo peel AC	680	[76]
Prosopis juliflora AC	10	[77]
Corncob AC	38	[78]
Waste cellulose	337	[79]
Acacia mangium wood AC	7.54	[80]
Bottom ash	3.61	[12]
De-oiled soya	1.66	[12]
Halloysite nanotubes (HNTs)	13.56	[8]
Lala clam shell	0.21	[13]
Bentonite	118	[33]
Modified cellulose	16.94	[31]
JFL AC	833	This study

Table 3
Adsorption kinetics parameters for MO adsorption on JFL AC

		Pseudo-first-order				Pseudo-second-order			
C_0 (mg/L)	q_{exp}	k_1	q_e	R^2	χ^2	k_2	q_e	R^2	χ^2
100	140	0.0119	130.27	0.9078		0.00028	144.93	0.9921	
150	170	0.0147	82.69	0.9903		0.00045	175.44	0.9983	
200	242	0.0116	121.99	0.9509	842.27	0.00023	250	0.9968	1.33
250	280	0.0181	170.13	0.987		0.00022	294.12	0.9971	
300	318	0.0113	91.53	0.9574		0.00027	322.58	0.9982	

from dye loaded adsorbent. At first, adsorption test was conducted at pH 3 (C_0 = 300 mg/L, V = 200 mL, W = 0.1 g). Thereafter, the adsorbent was separated from the solution and dried in an oven at 70°C for 12 h. Desorption of dye from the adsorbent was achieved by immersing the dye loaded adsorbent in 200 mL distilled water adjusted to pH 9. The amount of dye desorbed was estimated from the dye solution concentration after desorption. The dye recovery ratio was calculated as:

$$\text{Recovery ratio} = \frac{\text{Amount of dye desorbed}}{\text{Amount of dye adsorbed}} \quad (11)$$

The dye recovery ratio was found to be 0.759, which meant that 75.9% of the adsorbed dye could be recovered by simply swing the solution pH to 9. The adsorbent after desorption experiment was separated by centrifugation, washed with distilled water and dried in an oven at 70°C for 12 h. Because to the deportation interaction with hydroxyl groups, the surface of AC becomes negatively charged when the pH is raised. As a result of the negatively charged surface, the repulsion force between the adsorbent surface and the anionic dye molecule increased, resulting in a decrease in adsorption as predicted in Eq. (11).

$$\text{AC-OH}_2^+ \cdots \text{MO} + 2\text{OH}^- \rightarrow \text{AC-O}^- + 2\text{H}_2\text{O} + \text{MO} \quad (12)$$

The adsorption test was then repeated using the regenerated adsorbent and MO dye solution (pH 3, C_0 = 300 mg/L, V = 200 mL, W = 0.1 g)). It was founded that the dye removal percentages were 53% and 40.16% for fresh and regenerated JFL AC, respectively for the studied experimental conditions. The dye removal percentage decreased by 12.84% in case of regenerated JFL AC. Therefore, the prepared activated carbon is reusable.

3.2.8. Thermodynamic study

The adsorption thermodynamic parameters, such as change in Gibbs free energy ($\Delta G°$, kJ/mol), enthalpy ($\Delta H°$, kJ/mol), and entropy ($\Delta S°$, J/mol K) were evaluated using the following equations [81]:

$$\Delta G° = -RT \ln K_d \quad (13)$$

$$\ln K_d = \frac{\Delta S°}{R} - \frac{\Delta H°}{RT} \quad (14)$$

where R (8.314 J/mol K) is the universal gas constant, T (K) is the absolute solution temperature and K_d is the distribution coefficient defined as:

$$K_d = \frac{q_e}{C_e} \quad (15)$$

The values of $\Delta H°$ and $\Delta S°$ were estimated from the slope and intercept of the linear plot of $\ln K_d$ vs. $1/T$ (Fig. 8) for MO initial concentration of 300 mg/L. The calculated values of $\Delta G°$, $\Delta H°$, and $\Delta S°$ are presented in Table 4.

The negative values of $\Delta G°$ (Table 4) suggest that the adsorption of MO onto JFL AC is spontaneous and feasible [81]. The positive value of $\Delta S°$ implies the higher disorder of the adsorption system, possibly due to the redistribution of energy between the MO dye and JFL AC adsorbent during the adsorption process. In addition, positive value of $\Delta H°$ indicates the endothermic nature of

Table 4
Thermodynamic parameters for the removal of MO onto JFL AC

T (K)	$\Delta G°$ (kJ/mol)	$\Delta H°$ (kJ/mol)	$\Delta S°$ (J/(mol K))
308	–2.295		
301	–2.035	9.127	37.08
294	–1.776		

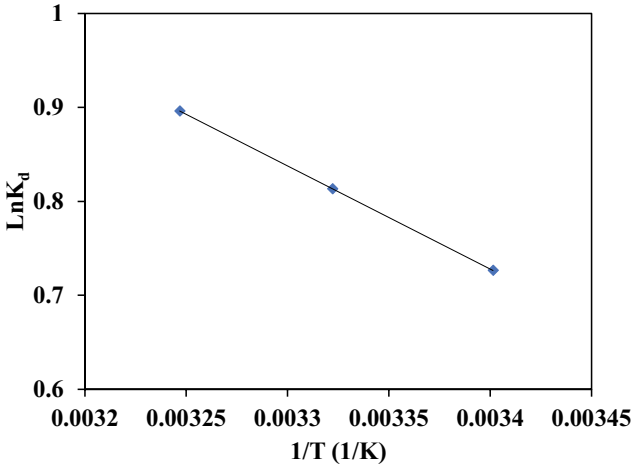

Fig. 8. Plot of $\ln K_d$ vs. $1/T$ for the adsorption of MO onto JFL AC adsorbent.

MO adsorption [82]. Similar result was reported for the adsorption of Procion Red dye on activated carbon [83].

4. Conclusion

The AC was prepared from low cost and locally available jackfruit leaves. The ability of the prepared AC to adsorb MO from aqueous solution was inspected in batch mode. The N_2 adsorption–desorption isotherm confirmed the mesoporous structure of the prepared AC with surface area of 81.45 m^2/g. The MO dye was found to adsorb strongly on the surface of the AC. The amount of dye adsorbed was found to vary with initial solution pH, initial dye concentrations and contact time. The adsorption of MO onto prepared AC was favorable in lower pH. The adsorption capacity (mg/g) was increased with increasing initial solution concentration. The adsorption process was found to follow pseudo-second-order kinetic model. Equilibrium data fitted very well to the Langmuir isotherm equation, demonstrating MO monolayer adsorption onto JFL AC with a monolayer adsorption capacity of 833 mg/g, which was higher than AC generated from numerous low-cost sources described in the literature. The AC prepared from jackfruit leaves is expected to be an effective, economically viable and promising adsorbent for the removal of MO from aqueous solutions.

Author contributions

M.Z.B (Professor) helped in carrying out experiment and assist in calculations, drawings and interpretation. S. H. (Lecturer) wrote the manuscript. M.A. (Lecturer) conducted experiment and helped drafted the manuscript. M.T. (Professor) provided the intellectual input and the protocols to be followed in the study, lead the overall study and critically revised the manuscript (corresponding author).

Acknowledgements

The Shahjalal University of Science and Technology (SUST) Research Grant, 2018 (Project ID.: SUST/2016/AS/02) for conducting this research work is highly appreciated.

Conflict of interest

On behalf of all authors, the corresponding author states that there is no conflict of interest.

References

[1] H.A. Shindy, Fundamentals in the chemistry of cyanine dyes: a review, Dyes Pigm., 145 (2017) 505–513.
[2] Md. Tamez Uddin, Md. Arifur Rahman, Md. Rukanuzzaman, Md. Akhtarul Islam, A potential low cost adsorbent for the removal of cationic dyes from aqueous solutions, Appl. Water Sci., 7 (2017) 2831–2842.
[3] K.-C. Chen, J.-Y. Wu, D.-J. Liou, S.-C. John Hwang, Decolorization of the textile dyes by newly isolated bacterial strains, J. Biotechnol., 101 (2003) 57–68.
[4] Z. Noorimotlagh, R. Darvishi Cheshmeh Soltani, A.R. Khataee, S. Shahriyar, H. Nourmoradi, Adsorption of a textile dye in aqueous phase using mesoporous activated carbon prepared from Iranian milk vetch, J. Taiwan Inst. Chem. Eng., 45 (2014) 1783–1791.
[5] M.M.R. Khan, M.Z.B. Mukhlish, M.S.I. Mazumder, K. Ferdous, D.M.R. Prasad, Z. Hassan, Uptake of Indosol Dark-blue GL dye from aqueous solution by water hyacinth roots powder: adsorption and desorption study, Int. J. Environ. Sci. Technol., 11 (2014) 1027–1034.
[6] M.Z. Bin Mukhlish, Y. Horie, T. Nomiyama, Flexible alumina-silica nanofibrous membrane and its high adaptability in Reactive Red-120 dye removal from water, Water Air Soil Pollut., 228 (2017), doi: 10.1007/s11270-017-3546-7.
[7] M.S. Tsuboy, J.P.F. Angeli, M.S. Mantovani, S. Knasmüller, G.A. Umbuzeiro, L.R. Ribeiro, Genotoxic, mutagenic and cytotoxic effects of the commercial dye CI Disperse Blue 291 in the human hepatic cell line HepG2, Toxicol. In Vitro, 21 (2007) 1650–1655.
[8] L. Wu, X. Liu, G. Lv, R. Zhu, L. Tian, M. Liu, Y. Li, W. Rao, T. Liu, L. Liao, Study on the adsorption properties of methyl orange by natural one-dimensional nano-mineral materials with different structures, Sci. Rep., 11 (2021), doi: 10.1038/s41598-021-90235-1.
[9] J. Mittal, Permissible synthetic food dyes in India, Resonance, 25 (2020) 567–577.
[10] M. Imran, D.E. Crowley, A. Khalid, S. Hussain, M.W. Mumtaz, M. Arshad, Microbial biotechnology for decolorization of textile wastewaters, Rev. Environ. Sci. Biotechnol., 14 (2015) 73–92.
[11] M.T. Uddin, M.Z. Bin Mukhlish, M.R.H. Patwary, A novel magnetically separable $CoFe_2O_4/SnO_2$ composite photocatalyst for the degradation of methylene blue dye from aqueous solution, Desal. Water Treat., 212 (2021) 311–322.
[12] A. Mittal, A. Malviya, D. Kaur, J. Mittal, L. Kurup, Studies on the adsorption kinetics and isotherms for the removal and recovery of Methyl Orange from wastewaters using waste materials, J. Hazard. Mater., 148 (2007) 229–240.
[13] A.A.A. Eljiedi, A. Kamari, Removal of methyl orange and methylene blue dyes from aqueous solution using lala clam (*Orbicularia orbiculata*) shell, AIP Conf. Proc., 1847 (2017) 040003, doi: 10.1063/1.4983899.
[14] M.T. Uddin, M.A. Islam, S. Mahmud, M. Rukanuzzaman, Adsorptive removal of methylene blue by tea waste, J. Hazard. Mater., 164 (2009) 53–60.
[15] M. Ahmadzadeh Tofighy, T. Mohammadi, Methylene blue adsorption onto granular activated carbon prepared from Harmal seeds residue, Desal. Water Treat., 52 (2014) 2643–2653.
[16] J. Shou, M. Qiu, Adsorption kinetics of phenol in aqueous solution onto activated carbon from wheat straw lignin, Desal. Water Treat., 57 (2016) 3119–3124.
[17] E. Ellouze, D. Ellouze, A. Jrad, R. Ben Amar, Treatment of synthetic textile wastewater by combined chemical coagulation/membrane processes, Desal. Water Treat., 33 (2011) 118–124.
[18] C.Y. Teh, P.M. Budiman, K.P.Y. Shak, T.Y. Wu, Recent advancement of coagulation-flocculation and its application in wastewater treatment, Ind. Eng. Chem. Res., 55 (2016) 4363–4389.
[19] M.T. Uddin, Y. Nicolas, C. Olivier, L. Servant, T. Toupance, S. Li, A. Klein, W. Jaegermann, Improved photocatalytic activity in RuO_2-ZnO nanoparticulate heterostructures due to inhomogeneous space charge effects, Phys. Chem. Chem. Phys., 17 (2015) 5090–5102.
[20] M.T. Uddin, Y. Sultana, M.A. Islam, Nano-sized SnO_2 photocatalysts: synthesis, characterization and their application for the degradation of Methylene Blue dye, J. Sci. Res., 8 (2016) 399, doi: 10.3329/jsr.v8i3.27524.
[21] M.T. Uddin, M.Z.B. Mukhlish, M.R.H. Patwary, A novel magnetically separable $CoFe_2O_4/SnO_2$ composite photocatalyst for the degradation of methylene blue dye from aqueous solution, Desal. Water Treat., 212 (2021) 311–322.
[22] N. Hu, W. Liu, L. Ding, Z. Wu, H. Yin, D. Huang, H. Li, L. Jin, H. Zheng, Removal of methylene blue from its aqueous solution by froth flotation: hydrophobic silica nanoparticle as a collector, J. Nanopart. Res., 19 (2017), doi: 10.1007/s11051-017-3762-5.
[23] E.K. Morali, N. Uzal, U. Yetis, Ozonation pre and post-treatment of denim textile mill effluents: Effect of cleaner production measures, J. Cleaner Prod., 137 (2016) 1–9.

[24] E. Kurt, D.Y. Koseoglu-Imer, N. Dizge, S. Chellam, I. Koyuncu, Pilot-scale evaluation of nanofiltration and reverse osmosis for process reuse of segregated textile dyewash wastewater, Desalination, 302 (2012) 24–32.
[25] E. Sahinkaya, S. Tuncman, I. Koc, A.R. Guner, S. Ciftci, A. Aygun, S. Sengul, Performance of a pilot-scale reverse osmosis process for water recovery from biologically-treated textile wastewater, J. Environ. Manage., 249 (2019) 109382, doi: 10.1016/j.jenvman.2019.109382.
[26] S.A. Mirbagheri, A. Charkhestani, Pilot-scale treatment of textile wastewater by combined biological-adsorption process, Desal. Water Treat., 57 (2016) 9082–9092.
[27] K. Singh, S. Arora, Removal of synthetic textile dyes from wastewaters: a critical review on present treatment technologies, Crit. Rev. Env. Sci. Technol., 41 (2011) 807–878.
[28] M. Tamez Uddin, M. Rukanuzzaman, M. Maksudur Rahman Khan, M. Akhtarul Islam, Adsorption of methylene blue from aqueous solution by jackfruit (*Artocarpus heteropyllus*) leaf powder: a fixed-bed column study, J. Environ. Manage., 90 (2009) 3443–3450.
[29] J. Mittal, R. Ahmad, A. Mittal, Kahwa tea (*Camellia sinensis*) carbon — a novel and green low-cost adsorbent for the sequestration of titan yellow dye from its aqueous solutions, Desal. Water Treat., 227 (2021) 404–411.
[30] M.Z. Bin Mukhlish, M.R. Khan, M.C. Bhoumick, S. Paul, Papaya (*Carica papaya* L.) leaf powder: novel adsorbent for removal of methylene blue from aqueous solution, Water Air Soil Pollut., 223 (2012) 4949–4958.
[31] R. Lafi, L. Abdellaoui, I. Montasser, A. Hafiane, Removal of methyl orange from aqueous solution onto modified extracted cellulose from *Stipa Tenacissima* L, Int. J. Environ. Anal. Chem., (2020), doi: 10.1080/03067319.2020.1845663.
[32] J.M. Yang, R.J. Ying, C.X. Han, Q.T. Hu, H.M. Xu, J.H. Li, Q. Wang, W. Zhang, Adsorptive removal of organic dyes from aqueous solution by a Zr-based metal-organic framework: effects of Ce(III) doping, Dalton Trans., 47 (2018) 3913–3920.
[33] A. Bellifa, M. Makhlouf, Z.H. Boumila, Comparative study of the adsorption of methyl orange by bentonite and activated carbon, Acta Phys. Pol. A, 132 (2017) 466–468.
[34] A. Mariyam, J. Mittal, F. Sakina, R.T. Baker, A.K. Sharma, Adsorption behaviour of Chrysoidine R dye on a metal/halide-free variant of ordered mesoporous carbon, Desal. Water Treat., 223 (2021) 425–433.
[35] V.K. Gupta, S. Agarwal, R. Ahmad, A. Mirza, J. Mittal, Sequestration of toxic congo red dye from aqueous solution using ecofriendly guar gum/ activated carbon nanocomposite, Int. J. Biol. Macromol., 158 (2020) 1310–1318.
[36] A. Patel, S. Soni, J. Mittal, A. Mittal, C. Arora, Sequestration of crystal violet from aqueous solution using ash of black turmeric rhizome, Desal. Water Treat., 220 (2021) 342–352.
[37] V.K. Gupta, A. Nayak, B. Bhushan, S. Agarwal, A critical analysis on the efficiency of activated carbons from low-cost precursors for heavy metals remediation, Crit. Rev. Env. Sci. Technol., 45 (2015) 613–668.
[38] O. Ioannidou, A. Zabaniotou, Agricultural residues as precursors for activated carbon production—a review, Renewable Sustainable Energy Rev., 11 (2007) 1966–2005.
[39] M.A. Yahya, Z. Al-Qodah, C.W.Z. Ngah, Agricultural bio-waste materials as potential sustainable precursors used for activated carbon production: a review, Renewable Sustainable Energy Rev., 46 (2015) 218–235.
[40] G.E. Sharaf El-Deen, S.E.A. Sharaf El-Deen, Kinetic and isotherm studies for adsorption of Pb(II) from aqueous solution onto coconut shell activated carbon, Desal. Water Treat., 57 (2016) 28910–28931.
[41] T.H. Liou, S.J. Wu, Characteristics of microporous/mesoporous carbons prepared from rice husk under base- and acid-treated conditions, J. Hazard. Mater., 171 (2009) 693–703.
[42] J. Saleem, U. Bin Shahid, M. Hijab, H. Mackey, G. McKay, Production and applications of activated carbons as adsorbents from olive stones, Biomass Convers. Biorefin., 9 (2019) 775–802.
[43] D. Özçimen, A. Ersoy-Meriçboyu, Adsorption of copper(II) ions onto hazelnut shell and apricot stone activated carbons, Adsorpt. Sci. Technol., 28 (2010) 327–340.
[44] N. Yadav, D.N. Maddheshiaya, S. Rawat, J. Singh, Adsorption and equilibrium studies of phenol and para-nitrophenol by magnetic activated carbon synthesised from cauliflower waste, Environ. Eng. Res., 25 (2020) 742–752.
[45] J. Zhang, Q. Zhou, L. Ou, Removal of indigo carmine from aqueous solution by microwave-treated activated carbon from peanut shell, Desal. Water Treat., 57 (2016) 718–727.
[46] K.J. Cronje, K. Chetty, M. Carsky, J.N. Sahu, B.C. Meikap, Optimization of chromium(VI) sorption potential using developed activated carbon from sugarcane bagasse with chemical activation by zinc chloride, Desalination, 275 (2011) 276–284.
[47] N. Bouchemal, Y. Azoudj, Z. Merzougui, F. Addoun, Adsorption modeling of orange G dye on mesoporous activated carbon prepared from algerian date pits using experimental designs, Desal. Water Treat., 45 (2012) 284–290.
[48] L. Wang, Adsorption of Direct Blend Yellow D-3RNL onto bamboo-base activated carbon: optimization, kinetics, and isotherm, Desal. Water Treat., 51 (2013) 5792–5804.
[49] D. Prahas, Y. Kartika, N. Indraswati, S. Ismadji, Activated carbon from jackfruit peel waste by H_3PO_4 chemical activation: pore structure and surface chemistry characterization, Chem. Eng. J., 140 (2008) 32–42.
[50] K.Y. Foo, L.K. Lee, B.H. Hameed, Preparation of activated carbon from sugarcane bagasse by microwave assisted activation for the remediation of semi-aerobic landfill leachate, Bioresour. Technol., 134 (2013) 166–172.
[51] T. Ahmed, W. Noor, O. Faruk, M.C. Bhoumick, M.T. Uddin, Removal of methylene blue (MB) from waste water by adsorption on jackfruit leaf powder (JLP) in continuously stirred tank reactor, J. Phys. Conf. Ser., 1086 (2018) 012012, doi: 10.1088/1742-6596/1086/1/012012.
[52] S. Jain, R. V. Jayaram, Adsorption of phenol and substituted chlorophenols from aqueous solution by activated carbon prepared from jackfruit (*Artocarpus heterophyllus*) peel-kinetics and equilibrium studies, Sep. Sci. Technol., 42 (2007) 2019–2032.
[53] B.S. Inbaraj, N. Sulochana, Use of jackfruit peel carbon (JPC) for adsorption of Rhodamine-B, a basic dye from aqueous solution, Indian J. Chem. Technol., 13 (2006) 17–23.
[54] B.S. Inbaraj, N. Sulochana, Carbonised jackfruit peel as an adsorbent for the removal of Cd(II) from aqueous solution, Bioresour. Technol., 94 (2004) 49–52.
[55] S. Khamparia, D. Jaspal, Investigation of adsorption of Rhodamine B onto a natural adsorbent Argemone mexicana, J. Environ. Manage., 183 (2016) 786–793.
[56] I. Langmuir, The constitution and fundamental properties of solids and liquids. Part I. Solids, J. Am. Chem. Soc., 38 (1916) 2221–2295.
[57] H.M.F. Freundlich, Uber die adsorption in Lasugen, J. Phys. Chem., 57 (1906) 385–470.
[58] K. Fytianos, E. Voudrias, E. Kokkalis, Sorption–desorption behaviour of 2,4-dichlorophenol by marine sediments, Chemosphere, 40 (2000) 3–6.
[59] S.K. Lagergren, About the theory of so-called adsorption of soluble substances, Sven. Vetenskapsakad. Handingarl., 24 (1898) 1–39.
[60] Y.S. Ho, G. McKay, Pseudo-second-order model for sorption processes, Process Biochem., 34 (1999) 451–465.
[61] A. Barroso-Bogeat, M. Alexandre-Franco, C. Fernández-González, V. Gómez-Serrano, FTIR analysis of pyrone and chromene structures in activated carbon, Energy Fuels, 28 (2014) 4096–4103.
[62] T. Jiang, Y.D. Liang, Y.J. He, Q. Wang, Activated carbon/$NiFe_2O_4$ magnetic composite: a magnetic adsorbent for the adsorption of methyl orange, J. Environ. Chem. Eng., 3 (2015) 1740–1751.
[63] H. Chen, J. Zhao, J. Wu, G. Dai, Isotherm, thermodynamic, kinetics and adsorption mechanism studies of methyl orange by surfactant modified silkworm exuviae, J. Hazard. Mater., 192 (2011) 246–254.

[64] K.S.W. Sing, D.H. Everett, R.A.W. Haul, L. Moscou, R.A. Pierotti, J. Rouquerol, T. Siemieniewska, Reporting physisorption data for gas/solid systems with special reference to the determination of surface area and porosity, Pure Appl. Chem., 57 (1985) 603–619.
[65] E.P. Barrett, L.G. Joyner, P.P. Halenda, The determination of pore volume and area distributions in porous substances. I. Computations from nitrogen isotherms, J. Am. Chem. Soc., 73 (1951) 373–380.
[66] T. Uddin, Rukanuzzaman, M. Rahman Khan, A. Islam, Jackfruit (*Artocarpus heterophyllus*) leaf powder: an effective adsorbent for removal of methylene blue from aqueous solutions, Indian J. Chem. Technol., 16 (2009) 142–149.
[67] H.O. Chukwuemeka-Okorie, F.K. Ekuma, K.G. Akpomie, J.C. Nnaji, A.G. Okereafor, Adsorption of tartrazine and sunset yellow anionic dyes onto activated carbon derived from cassava sievate biomass, Appl. Water Sci., 11 (2021), doi: 10.1007/s13201-021-01357-w.
[68] M. Küçükosmanoğlu, O. Gezici, A. Ayar, The adsorption behaviors of Methylene Blue and Methyl Orange in a diaminoethane sporopollenin-mediated column system, Sep. Purif. Technol., 52 (2006) 280–287.
[69] S. Rattanapan, J. Srikram, P. Kongsune, Adsorption of Methyl Orange on coffee grounds activated carbon, Energy Procedia, 138 (2017) 949–954, doi: 10.1016/j.egypro.2017.10.064.
[70] S. Chen, J. Zhang, C. Zhang, Q. Yue, Y. Li, C. Li, Equilibrium and kinetic studies of methyl orange and methyl violet adsorption on activated carbon derived from *Phragmites australis*, Desalination, 252 (2010) 149–156.
[71] M.R. Samarghandi, M. Hadi, S. Moayedi, F.B. Askari, Two-parameter isotherms of methyl orange sorption by pinecone derived activated carbon, Iran. J. Environ. Health Sci. Eng., 6 (2009) 285–294.
[72] R. Gong, J. Ye, W. Dai, X. Yan, J. Hu, X. Hu, S. Li, H. Huang, Adsorptive removal of methyl orange and methylene blue from aqueous solution with finger-citron-residue-based activated carbon, Ind. Eng. Chem. Res., 52 (2013) 14297–14303.
[73] K. Mahmoudi, K. Hosni, N. Hamdi, E. Srasra, Kinetics and equilibrium studies on removal of methylene blue and methyl orange by adsorption onto activated carbon prepared from date pits–a comparative study, Korean J. Chem. Eng., 32 (2014) 274–283.
[74] X. Tao, Y. Wu, L. Cha, Shaddock peels-based activated carbon as cost-saving adsorbents for efficient removal of Cr(VI) and methyl orange, Environ. Sci. Pollut. Res., 26 (2019) 19828–19842.
[75] M.B. Alqaragully, Removal of textile dyes (Maxilon Blue, and Methyl Orange) by date stones activated carbon, Int. J. Adv. Res. Chem. Sci., 1 (2014) 48–59.
[76] H. Li, Z. Sun, L. Zhang, Y. Tian, G. Cui, S. Yan, A cost-effective porous carbon derived from pomelo peel for the removal of methyl orange from aqueous solution, Colloids Surf., A, 489 (2016) 191–199.
[77] M. Kumar, R. Tamilarasan, Modeling of experimental data for the adsorption of methyl orange from aqueous solution using a low cost activated carbon prepared from prosopis julifl ora, Polish J. Chem. Technol., 15 (2013) 29–39.
[78] X.X. Hou, Q.F. Deng, T.Z. Ren, Z.Y. Yuan, Adsorption of Cu^{2+} and methyl orange from aqueous solutions by activated carbons of corncob-derived char wastes, Environ. Sci. Pollut. Res., 20 (2013) 8521–8534.
[79] B. Sun, Y. Yuan, H. Li, X. Li, C. Zhang, F. Guo, X. Liu, K. Wang, X.S. Zhao, Waste-cellulose-derived porous carbon adsorbents for methyl orange removal, Chem. Eng. J., 371 (2019) 55–63.
[80] M. Danish, R. Hashim, M.N.M. Ibrahim, O. Sulaiman, Characterization of physically activated *Acacia mangium* wood-based carbon for the removal of methyl orange dye, BioResources, 8 (2013) 4323–4339.
[81] B.H. Hameed, A.A. Ahmad, N. Aziz, Adsorption of reactive dye on palm-oil industry waste: equilibrium, kinetic and thermodynamic studies, Desalination, 247 (2009) 551–560.
[82] A.R. Agcaoili, M.U. Herrera, C.M. Futalan, M.D.L. Balela, Fabrication of polyacrylonitrile-coated kapok hollow microtubes for adsorption of methyl orange and Cu(II) ions in aqueous solution, J. Taiwan Inst. Chem. Eng., 78 (2017) 359–369.
[83] M.R. Khan, M.M. Rahman, M.S.I. Mozumder, M.J. Uddin, M.A. Islam, Adsorption behavior of reactive dye from aqueous phase on activated carbon, Pol. J. Chem., 83 (2009) 1365–1378.

Supplementary information

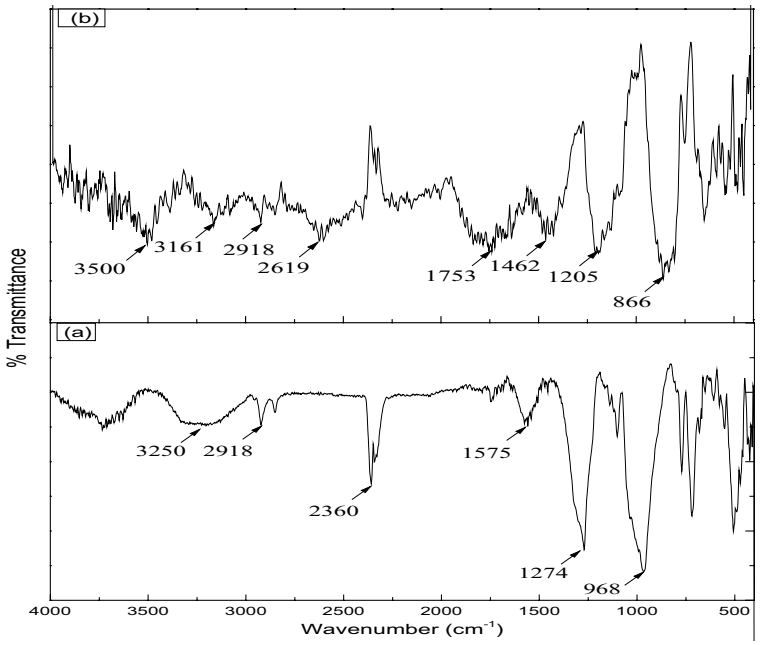

Fig. S1. FTIR spectra of JFL AC before (a) and after (b) adsorption of MO.

Point of zero charge, pH_{PZC}, is reported as the pH at which sum of all the surface positive charges balances sum of all the surface negative charges. The choice of working solution pH is strongly dependent on the pH_{PZC} as it influences the nature of interaction between the adsorbate and adsorbent. At a solution pH below pH_{PZC}, the surface of the sorbent becomes positively charged and attracts anions from the solution. Whereas, when the solution pH is greater than pH_{PZC}, the surface negativity increases and cations get increasingly attracted. The point of zero charge of JFL AC was determined to be 4.2 from pH_{final}–$pH_{initial}$ vs. $pH_{initial}$ plot as shown in Fig. S2.

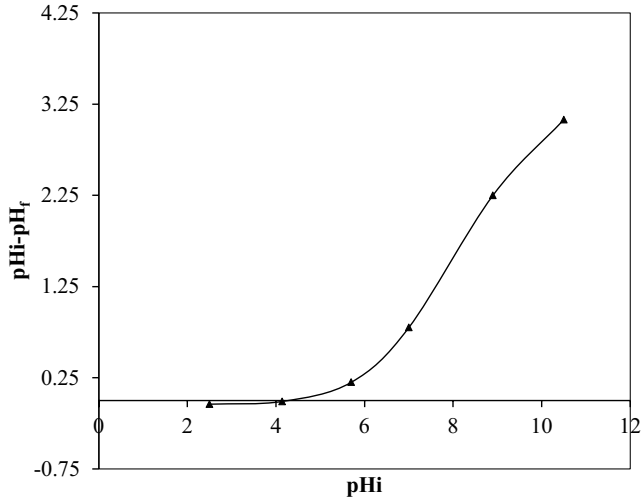

Fig. S2. Determination of point of zero charge.

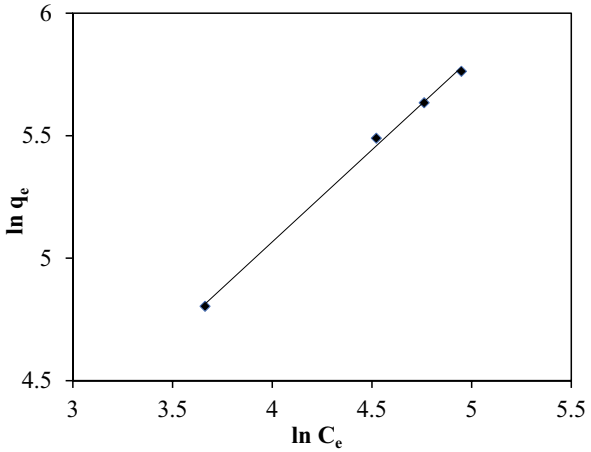

Fig. S3. Freundlich isotherm for adsorption of MO on JFL AC adsorbent (C_0 = 100, 200, 250 and 300 mg/L, W = 0.1 g, V = 200 mL, T = 28°C).

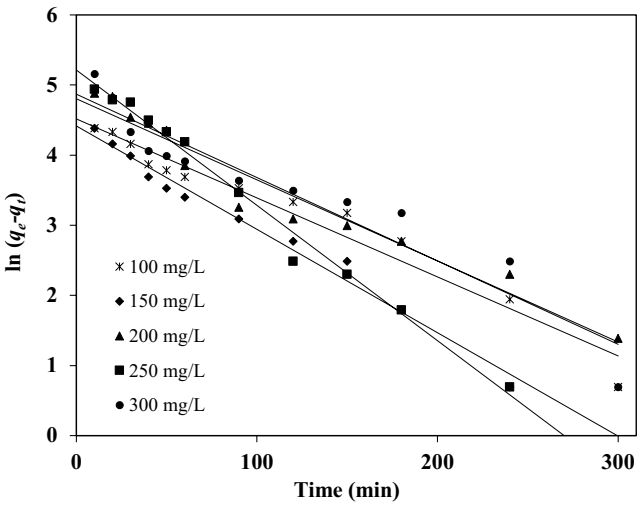

Fig. S4. Pseudo-first-order kinetic plot for the adsorption of MO onto JFL AC.